Journal of Engineering Mathematics **32:** 27–40, 1997.

Slow slumping of a very viscous liquid bridge

E.O. TUCK[1], Y.M. STOKES[1] and L.W. SCHWARTZ[2]
[1]*Applied Mathematics Department, The University of Adelaide, Adelaide, Australia 5005; e-mail: etuck@maths.adelaide.edu.au*
[2]*Department of Mechanical Engineering, University of Delaware, Newark, DE 19716, U.S.A.*

Received 17 October 1995; accepted in revised form 11 November 1996

Abstract. A layer of very viscous liquid (*e.g.* tar, molten glass) spans a chasm between two vertical walls. The slow fall or slump of this initially-rectangular liquid bridge is analysed. A semi-analytical solution is obtained for the initial motion, for arbitrary thickness/width ratios. The formal limits of large and small thickness/width ratios are also investigated. For example, the centre section of a thin bridge of liquid of density ρ and viscosity μ, with width $2w$ and thickness $2h \ll 2w$ falls under gravity g at an initial velocity $\rho g w^4/(32\mu h^2)$. A finite element technique is then employed to determine the slumping motion at later times, confirming in passing the semi-analytical prediction of the initial slumping velocity.

Key words: slumping, creeping flow, molten glass, Stokes flow, finite elements

1. Introduction

There are applications (*e.g.* in the optical industry for molten glass [1]) where a very viscous liquid is allowed to 'slump' under gravity. The motion is very slow, *e.g.* with a time scale of hours, and the boundary geometry of the liquid mass departs by only a small (though crucial to the application) amount from its original configuration during the motion. For example, modern multifocal spectacle lenses, with varying curvature, are sometimes produced by such slumping processes. Working temperatures are typically in the range of 500–750°C, for which the corresponding molten glass viscosities are of the order of $10^{14} - 10^6$ Pa.s ([2]). Incidentally, precise determination of the magnitude of such high viscosities presents practical difficulties ([3, 4], [5, p. 43]), and in addition to being relevant to the industrial process itself, the slumping rates predicted here, when compared with experimental results, may prove useful for viscosity measurement.

We consider here a very simple two-dimensional special case of such a slumping motion. The pre-moving (perhaps pre-melting) liquid mass is considered to be a rectangular $(2w \times 2h)$ strip across the gap between two vertical rigid walls, as in Figure 1(a). At time $t = 0$, the mass becomes a very viscous Newtonian liquid of viscosity μ, which then slumps in Stokes flow to a configuration as in Figure 1(b), while being retarded with no slip at the walls.

We ignore the effect of surface tension, *i.e.* we assume that the surface-tension coefficient σ for the fluids of interest is sufficiently small. A typical value for molten glass ([2, p. 24]) is $\sigma \approx 0{\cdot}3\text{Nm}^{-1}$. More precisely, neglect of surface tension is justified if the capillary number $\mu U/\sigma$ is large, where U is a typical slumping velocity. Since we shall find that in the present problem U scales as $\rho g w^2/\mu$, this capillary number scales as $\rho g w^2/\sigma$. For bridge dimensions w of the order of 10 cm or more, this yields adequately large values of capillary number, of the order of 10^3.

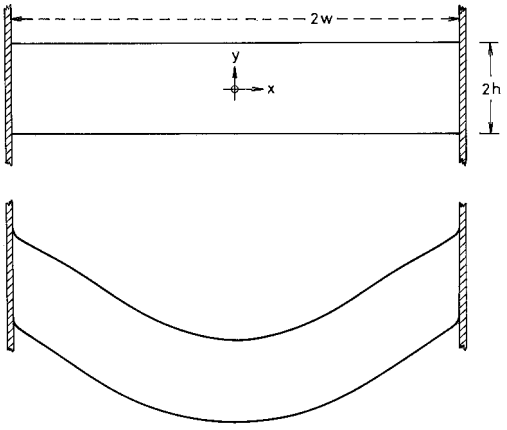

Figure 1. A slumping liquid bridge: (a) initially rectangular shape; (b) shape at a later time, when the bridge has slumped about one thickness.

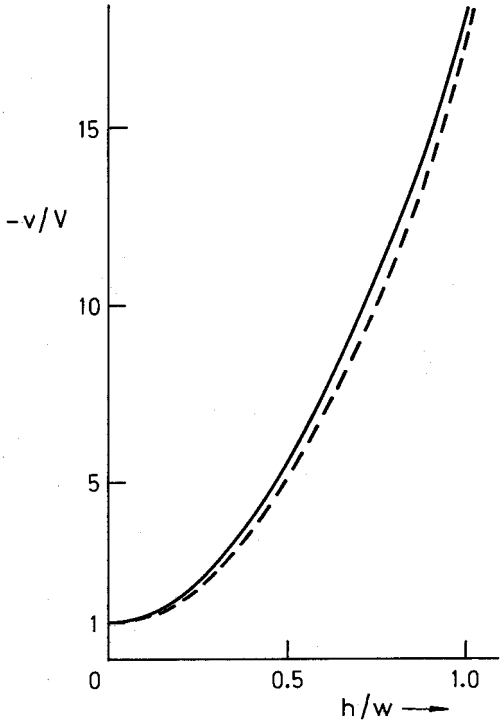

Figure 2. Initial slumping velocity $-v$, scaled with respect to the thin-bridge limit $V = \rho g w^4/(32\mu h^2)$, as a function of aspect ratio h/w. Solid curve is the velocity at the bridge centroid, dashed curve is the velocity at the free surface in the centre.

Let us assume that the upp er and lower free surfaces of the slumping mass are $y = \eta_\pm(x,t)$, respectively. Our task is to find these free surfaces as functions of time t, but because of the creeping nature of the flow, time plays only a parametric role. The initial rectangular domain has $\eta_\pm(x,0) = \pm h$. As the bridge slumps, its contact with the walls $x = \pm w$ remains fixed along $-h \leqslant y \leqslant h$ for all time; we assume that there is no slip down the walls, and the contact points at the corners $x = \pm w$, $y = \pm h$ do not move. Ultimately, some form of rupture must occur, but this is not considered in the present paper.

The assumption of Stokes flow, in which the inertia terms in the Navier–Stokes equations can be neglected, is justified by the huge viscosities of interest, leading to very low effective Reynolds numbers. This assumption also means that the flow appears to start not from rest, but rather with a non-zero initial velocity distribution. In practice, when the flow does start from rest, there is a transient situation occurring over a time scale comparable to that for development of a Stokes layer (*cf.* [6, p. 189]), in which layers of fluid distant w from an impulsively moved wall accelerate up to close to the wall velocity in a time of the order of $\rho w^2/\mu$. With the very large values of μ of interest here, this time is utterly negligible (*e.g.* milliseconds) relative to the slumping time (*e.g.* hours), and we can therefore assume that the initial velocity profile is developed instantaneously, in particular, before there is any departure of the free surface from its initial rectangular configuration. Determination of this initial impulsively-developed flow at time $t = 0_+$ is one of our primary aims in the present study.

The Stokes-flow assumption means that the full two-dimensional problem at all times is described by a stream function ψ satisfying the biharmonic equation

$$\nabla^4\psi = 0 \tag{1}$$

in the flow region $|x| < w,\ \eta_- < y < \eta_+$, where the fluid velocity is $(u, v) = (\psi_y, -\psi_x)$. On the vertical walls, we must have zero velocity, so

$$\psi_x = \psi_y = 0 \quad \text{on } x = \pm w. \tag{2}$$

The boundaries $y = \eta_\pm$ are free surfaces of zero stress, both normal and tangential. Formulas for the normal and tangential stresses are given by Wehausen and Laitone [7, p. 453]. In general, these are quite complicated expressions involving second derivatives of the stream function ψ, the pressure p, and the slopes $\eta' = \partial\eta_\pm/\partial x$ of the free surfaces. Namely for the normal stress we have

$$-p - 2\mu\frac{\psi_{xy}(1-\eta'^2) - (\psi_{xx} - \psi_{yy})\eta'}{1+\eta'^2} = 0 \tag{3}$$

and for the tangential stress

$$\mu\frac{(\psi_{xx} - \psi_{yy})(1-\eta'^2) + 4\psi_{xy}\eta'}{1+\eta'^2} = 0. \tag{4}$$

The pressure p must be obtained by integrating the Stokes equations ([6, p. 217]),

$$p_x = \mu\nabla^2\psi_y \tag{5}$$

and

$$p_y = -\rho g - \mu\nabla^2\psi_x. \tag{6}$$

At the initial instant $t = 0_+$, before sensible slumping has occurred, and while the geometry of the bridge remains rectangular with $\eta' = 0$, the normal stress condition (3) simplifies to

$$-p - 2\mu\psi_{xy} = 0 \tag{7}$$

and the tangential stress condition (4) to

$$\psi_{xx} - \psi_{yy} = 0. \tag{8}$$

Equation (7) can be differentiated tangentially (*i.e.* with respect to x at the initial instant) and (5) then used to eliminate the pressure, yielding

$$\psi_{yyy} + 3\psi_{xxy} = 0. \tag{9}$$

However, as we shall see, it is important in some parts of the solution process to retain the undifferentiated form of the normal-stress condition.

Gravity g is the forcing agent for this flow, and enters the problem via the y-component (6) of the Stokes equation, adding a hydrostatic term $-\rho g y$ to the pressure p. This term is lost in the differentiation of (7) to give (9), which is why we must use (7) itself at least once in the solution process. It is appropriate at this point to note that slumping could be induced not only by actual gravity, but also by an imposed pressure difference P between top and bottom free

surfaces, *c.f.* [8]. For example, at the initial instant $t = 0_+$, if the zero value for the normal stress is replaced by $T_n = \mp P/2$ on $y = \pm h$, it is easy to show that we get the same result by replacing actual gravity g by apparent gravity $g + P/(2\rho h)$, and retaining a zero normal stress condition. Although this equivalence no longer holds at later times, we shall from now on assume that the only forcing influence is due to (real or apparent) gravity.

Our task in the general time-dependent case is to solve (1) subject to the boundary conditions (2) on the walls, and (3, 4) on the free surfaces. The final boundary condition, ultimately allowing determination of the shapes of these free surfaces, is the kinematic condition

$$\frac{\partial \eta_\pm}{\partial t} + \psi_y \frac{\partial \eta_\pm}{\partial x} + \psi_x = 0. \tag{10}$$

Before discussing this time-dependent problem, we first solve for the initial impulsively-developed motion at $t = 0_+$, when the free surfaces are still essentially horizontal. Because of the rectangular geometry, this boundary-value problem is quite suitable for numerical methods such as finite differences, and that technique has indeed been used (with successive over-relaxation [9]) on some test cases, giving results in agreement with those to be described below. However, the present problem is very similar to elastic beam and plate problems, and a somewhat more efficient route to numerical results is via an eigenfunction expansion of a type very similar to those used in that field ([10, p. 35 ff.]).

2. Initial motion

We represent the stream function in the form of the series:

$$\begin{aligned}\frac{32h^2\mu}{\rho g}\psi \;=\; & \tfrac{1}{5}x^5 + 2x^3y^2 - 3xy^4 + 24h^2xy^2 \\ & + A_0 w^4 x + B_0 w^2 (\tfrac{1}{3}x^3 + xy^2) \\ & + w^5 \Re \sum_{j=1}^{\infty} C_j \left[\cos k_j \cos(k_j y/h) + \frac{y}{h} \sin k_j \sin(k_j y/h)\right] \frac{\sinh(k_j x/h)}{\sinh(k_j w/h)},\end{aligned} \tag{11}$$

where A_0 and B_0 are non-dimensional real constants to be determined, and $C_j = A_j + \mathrm{i}B_j$, $j = 1, 2, \ldots$, is an infinite set of non-dimensional complex constants to be determined. The eigenvalues k_j in (11) are solutions of the transcendental equation

$$\sin 2k = 2k, \tag{12}$$

which (see [11]) has infinitely many complex roots $k = k_j$, the first three of which are

$$k_1 = 3{\cdot}7488 + \mathrm{i}\,1{\cdot}3843,$$
$$k_2 = 6{\cdot}9500 + \mathrm{i}\,1{\cdot}6761,$$
$$k_3 = 10{\cdot}1193 + \mathrm{i}\,1{\cdot}8584.$$

The expansion (11) has the following justification and motivation. All terms have the required symmetries about $x = 0$ and $y = 0$, and satisfy the biharmonic equation (1) and

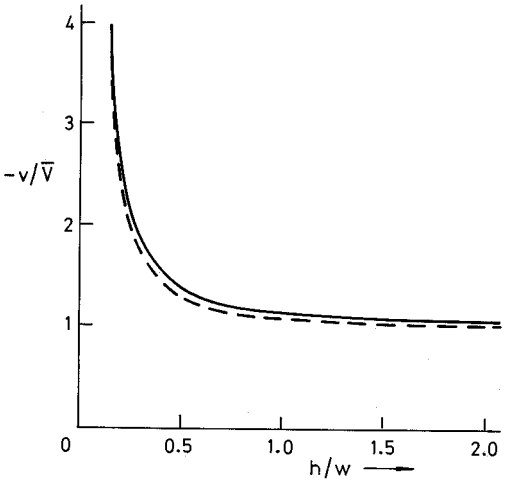

Figure 3. Same as Figure 2, except velocities scaled with respect to the (Poiseuille) thick-bridge limit $\bar{V} = \rho g w^2/(2\mu)$.

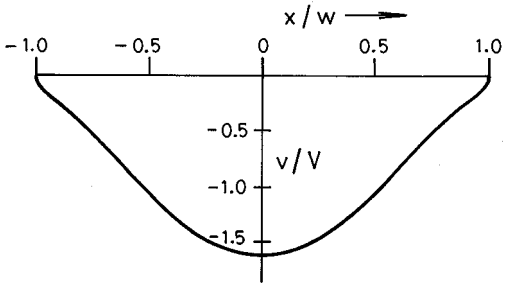

Figure 4. Variation across the bridge of the initial free-surface slumping velocity (also proportional to the initial free-surface deformation) at $h/w = 0{\cdot}2$.

the free-surface conditions (8, 9). The quintic polynomial on the first line is such that, on integrating (6) to provide the corresponding pressure field, we have

$$-p - 2\mu\psi_{xy} = \frac{\rho g}{2h^2} y(y^2 - h^2) \tag{13}$$

everywhere, which is independent of x, and vanishes on $y = \pm h$. Thus this part of (11) by itself satisfies the normal-stress condition in the undifferentiated form (7). This justifies the factor $32h^2\mu/(\rho g)$ multiplying ψ in (11), since none of the other terms in (11) contribute to the normal stress on $y = \pm h$.

The two terms on the second line of (11) represent, respectively, a vertical uniform stream of magnitude proportional to the unknown coefficient A_0 and a flow with a parabolic velocity profile of maximum velocity proportional to the unknown coefficient B_0. In any case, these terms generate zero normal and tangential stresses on any horizontal boundary.

Finally, the series on the third line of (11) is a sum of an infinite set of biharmonic eigenfunctions (see [12]), each of which separately satisfies the free-surface conditions (8, 9) providing that the eigenvalues k_j satisfy (12). None of the terms in the representation (11) satisfy the wall conditions (2). The terms in the series part of this representation can be considered as 'wall-correction' terms, since they are significant only when the ratio of hyperbolic sines is close to unity, and thus decay exponentially away from the walls $x = \pm w$.

All we have to do to complete solution of the problem is to choose the unknown real coefficients $\{A_j, B_j\}$, $j = 0, 1, 2, \ldots$, in order to satisfy the two wall conditions (2) at $x = \pm w$. If we truncate the series after N terms, and collocate these two wall conditions at $N + 1$ values of y, this leads to $2N + 2$ linear equations in $2N + 2$ unknowns $\{A_j, B_j\}$, $j = 0, 1, 2, \ldots, N$. The corresponding matrix is easy to write down and invert.

A typical output, shown in Figure 2 plotted against the aspect ratio h/w, is the downward slumping velocity $-v = \psi_x$, measured either at the centroid $(x, y) = (0, 0)$ of the liquid mass (solid curve), or at the corresponding point on the free surface $(x, y) = (0, \pm h)$ immediately above or below the centroid (dashed curve). The velocity at the free surface is generally about

5 to 10 percent lower than the velocity at the centroid. The scale for these slumping velocities is chosen in Figure 2 as

$$V = \frac{\rho g w^4}{32 \mu h^2}, \tag{14}$$

which is the small-h limit, to be discussed further below. These results were obtained with N taking values up to 80, by which time the value of v had converged to at least 3 significant figures.

When scaled with respect to its thin-bridge limit V as above, the slumping velocity increases rapidly with thickness. When h/w is large, the slumping velocity becomes asymptotically independent of thickness, and it is preferable to remove h from the velocity scale. Figure 3 replots the data of Figure 2 with a scale factor $\bar{V} = \rho g w^2/(2\mu)$, and indicates that the re-scaled slumping velocity is a decreasing function of h/w which tends to 1 as $h/w \to \infty$, a result which is also discussed below.

Figure 4 shows (for the representative value $h/w = 0{\cdot}2$) the variation $v(x, \pm h)/V$ across the bridge of the free-surface slumping velocity. This is an important output since the small-time integration of the kinematic boundary condition (8) predicts that the shape of the deforming surface is initially given by $y = \eta_{\pm} = \pm h + tv(x, \pm h)$. Note that this curve is somewhat bell-shaped, with significantly greater velocities near the centre of the bridge than near the walls (more so than would be the case for a parabolic profile), and with a final rapid decrease toward zero occurring in the last 5 percent of the distance from the wall.

This last effect can be explained by a corner-flow analysis (*c.f.* [13]). Suppose we take (r, θ) to be temporary local polar co-ordinates centered on $(x, y) = (-w, -h)$, where the lower free boundary corresponds to $\theta = 0$. The conditions of zero tangential and normal stress, equivalent to (7) and (8) then become

$$\psi_{rr} - \frac{1}{r}\psi_r - \frac{1}{r^2}\psi_{\theta\theta} = 0 \tag{15}$$

and

$$3\psi_{rr\theta} - \frac{3}{r}\psi_{r\theta} + \frac{4}{r^2}\psi_{\theta} - \frac{1}{r^2}\psi_{\theta\theta\theta} = 0, \tag{16}$$

respectively, on $\theta = 0$. An elementary biharmonic function satisfying these conditions is

$$\psi = r^{\lambda} F(\theta), \tag{17}$$

where

$$F(\theta) = A\left[\cos\lambda\theta - \frac{\lambda}{\lambda - 2}\cos(\lambda - 2)\theta\right] + B[\sin\lambda\theta - \sin(\lambda - 2)\theta]. \tag{18}$$

Nontrivial solutions for $F(\theta)$ that also obey (2), *i.e.* $F(\pi/2) = F'(\pi/2) = 0$, must have eigenvalues λ that satisfy

$$\sin(\lambda\pi/2) = \pm(\lambda - 1). \tag{19}$$

There is one real solution for each choice of sign in (19); for the velocity to be finite at the corner, the plus sign is chosen, and the corresponding root is $\lambda \approx 1{\cdot}5946$.

Since the vertical velocity v is proportional to the x-derivative of ψ, and $r \approx x + w$ on the free surface at the corner $x = -w$, we have thus shown that the free-surface value of v tends

to zero like $(1-|x|/w)^{0{\cdot}5946}$ as $x \to \pm w$, and its x-derivative becomes infinite. This mild singularity at the corners eventually slows convergence of both the eigenfunction expansion method and other numerical techniques such as finite difference or finite elements, but not catastrophically.

3. Limiting and extended results for thin and thick bridges

It is clear from the numerical results that in the thin-layer limit $h/w \to 0$, the coefficients C_j in the series part of the representation (11) tend to zero quite rapidly. These terms measure end effects near the walls. Their smallness for thin bridges is analogous to St.-Venant's principle in solid mechanics ([10, p. 33]), in the sense that in that limit, the details of the end attachments are not important, so long as certain gross measures are preserved.

In the present case, this leads to a simple heuristic asymptotic approximation, in which, having neglected the series portion of (11), we force the remaining terms to satisfy the wall conditions (2) to a first approximation in (small) y. In this way, we find immediately that $A_0 = 1$ and $B_0 = -2$, so that the limiting solution is just

$$\frac{32h^2\mu}{\rho g}\psi = \tfrac{1}{5}x^5 + w^4x - \tfrac{2}{3}w^2x^3 \tag{20}$$

to leading order. This represents a unidirectional flow with velocity profile

$$v = -V\left(1 - \frac{x^2}{w^2}\right)^2, \tag{21}$$

where V is given by (14), confirming that V is the limiting central slumping velocity, and indicating a 'parabolic-squared' bell-shaped velocity profile across the bridge. Our numerical results, such as those illustrated in Figure 4, confirm this profile as an outer expansion matching to a small 'edge layer' near the walls where the corner singularity discussed above plays a role.

The above is only a very *ad hoc* derivation of a thin-bridge result of some generality, analogous to thin-plate theory [14] in solid mechanics. In the Appendix, we provide an alternative derivation of a more general three-dimensional result, via a formal asymptotic expansion in powers of the small parameter h/w. The conclusion is that the leading-order approximation (for all $|y| < h$) to the initial vertical (upward) velocity v of a thin sheet whose boundaries are initially planes $y = \pm h$ satisfies the partial differential equation

$$\nabla^4 v = -\frac{3\rho g}{4\mu h^2} = \text{constant} \tag{22}$$

in the (x, z) plane. This is the same equation that describes deflection of a uniformly loaded thin elastic plate, provided v is re-interpreted as the deflection, and the viscosity μ is replaced by $E/(4(1-\nu^2))$, where E is Young's modulus and ν is Poisson's ratio (see also [4]). Equations describing movement of thin but non-planar viscous sheets are given in [8].

For fixed walls in the form of vertical cylinders with contour C in the (x, z)-plane, Equation (22) must be solved subject to the boundary conditions $v = v_n = 0$. If we specialize back to the two-dimensional case where C is $x = \pm w$, this yields (21) immediately, so verifying the *ad hoc* derivation via (20).

One of the valuable features of the thin-bridge limit is that it enables consideration of some more general geometries and physical assumptions. An example is the ability to solve (22) in

the three-dimensional case where C is a circle of radius w, for which we find that the centre velocity is $3/8$ths of that for a 2D channel of the same width.

A significant difference also results if the ends are less strongly fixed on the contour C. For example, we can retain the condition $v = 0$ of zero tangential velocity, but replace the condition $v_n = 0$ of zero normal velocity by a condition $v_{nn} = 0$ involving a double normal derivative, which can be shown to be equivalent in the thin-layer limit to vanishing of the stress component normal to C. When this is applied to the 2D case, we get

$$v = -V\left(1 - \frac{x^2}{w^2}\right)\left(5 - \frac{x^2}{w^2}\right). \tag{23}$$

Thus, when we allow flow normal to the walls at zero stress, the resulting centerline sag velocity is initially five times as great as that when normal flow is prevented.

It is also possible to do a 'thick-layer' asymptotic approximation for $h \gg w$. Again, only an *ad hoc* summary is attempted here. Namely, it appears that the flow approaches that of plane Poiseuille flow down the channel, with zero dynamic-pressure gradient. That is, the bridge falls as if it had no top or bottom free surface, driven solely by the hydrostatic pressure. That Poiseuille solution

$$v = -\frac{\rho g w^2}{2\mu}(1 - x^2/w^2) \tag{24}$$

has a parabolic profile with a centre slumping velocity $\bar{V} = \rho g w^2/(2\mu)$, thus confirming the numerical results as in Figure 3, in the large h/w limit. Thus, as the aspect ratio varies from $h/w = 0$ to $h/w = \infty$, the slumping profile across the bridge changes smoothly from parabolic-squared to parabolic.

4. Finite-element solutions

The above problem, both in its initial rectangular phase at $t = 0_+$, and especially at later times when there are non-trivial free surfaces $y = \eta_\pm(x, t)$, is very suitable for application of the finite-element technique. We have used a package called *Fastflo* ([15, 16]), as well as our own purpose-written finite-element program.

In setting up the problem for solution by finite elements, we feel that there is no particular advantage to be gained by using a streamfunction formulation, and retain primitive variables (u, v, p). The Stokes equations (5, 6) and the continuity equation

$$u_x + v_y = 0, \tag{25}$$

are combined as one matrix-vector operator equation. Our own program solves this fully-coupled system of equations directly for the three unknowns. However, within the *Fastflo* package, we use a 'penalty-method' approximation, in which the right-hand side of (25) is replaced by $-p/\alpha$, α being a large penalty factor [17]. This enables the pressure to be 'eliminated' from the equations and a new lower-order vector equation obtained in terms of velocity only. Once the velocity field has been determined, it can then be used if necessary to compute the pressure field, but we will not need to do this here.

Next, the (fully-coupled or penalty) problem is re-phrased in the standard variational manner, whereby the field equation, multiplied by an appropriate test function, is integrated over the flow domain, and Green's theorem used to replace terms involving second derivatives

Table 1. Slumping velocity at centroid

$h/w = 0{\cdot}2$			$h/w = 0{\cdot}5$		
# elements (1/4 domain)	Fully-coupled	Penalty (*Fastflo*)	# elements (1/4 domain)	Fully-coupled	Penalty (*Fastflo*)
154	1·673	1·668	164	5·395	5·391
243	1·674	1·672	252	5·396	5·391
337	1·674	1·673	342	5·396	5·388
426	1·674	1·673	436	5·397	5·396
511	1·674	1·672	536	5·397	5·396
608	1·674	1·674	634	5·398	5·396
707	1·674	1·674	728	5·398	5·397
			910	5·398	5·396
			1102	5·398	5·397
			1288	5·398	5·398
			1482		5·398

of velocities with terms involving first derivatives, plus boundary-integral terms. The latter are suitable for implementing the zero-stress boundary conditions on the free surfaces, while the test function is chosen to be zero on other boundaries having Dirichlet conditions, so that the net effect is to eliminate all boundary-integral contributions.

The flow domain was meshed with 6-node triangular elements by means of the *Fastflo* automatic mesh generator. When applying the penalty method which involves the velocity variables only, we used quadratic test functions, piecewise continuous between elements. For the solution of the fully-coupled problem which involves pressure as well as velocity variables, piecewise continuous linear test functions were used for the pressure, while quadratic test functions were used for the two velocity components. At the initial instant of time, though not subsequently, we are able to use symmetry to confine the computations to a quarter of the rectangle. For later times, there is only symmetry about the y-axis and we must solve the equations over a half of the flow domain. We used double-precision arithmetic and, where relevant, a penalty parameter α of the order of 10^4 was found to be adequate.

Considering first the initial solution in a rectangular domain, we have two independent finite-element solutions plus the solution of the eigenfunction expansion (11) which can be compared. For the two finite-element solutions, we have investigated convergence with respect to grid fineness for aspect ratios $h/w = 0{\cdot}2$ and $h/w = 0{\cdot}5$, using symmetry to restrict computation to a quarter of the rectangle, and varying the total number of triangular mesh elements between 150 and 1500. In view of the corner singularity, there is value in concentrating grid triangles near the corner, which can be done with appropriate input to the automatic grid generator, and in fact this is especially important when using the penalty method.

The centroid slumping velocities for the fully-coupled and penalty finite-element problems, for various numbers of mesh elements, with concentration at the corner, are given in Table 1. These clearly show convergence to at least three figures of accuracy, this accuracy being already attained with only a few hundred mesh elements. By contrast, when a uniform mesh was used in solving the fully-coupled system, more than 2000 mesh elements were required for similar accuracy, and the accuracy dropped even more markedly where a uniform mesh was used in conjunction with elimination of pressure by the penalty method.

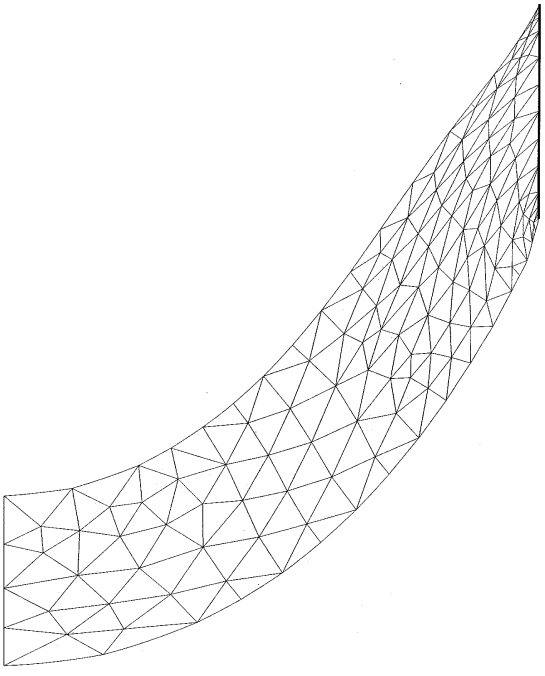

Figure 5. Slumped bridge with $h/w = 0{\cdot}2$ at time $t = 5{\cdot}0h/V$, when the slumping velocity is at about its minimum value.

The results given in Table 1 also agree to at least three figures with the solutions given by 80 or more terms of the eigenfunction expansion (11). For example, truncation of (11) to 80 terms gives centroid vertical velocities of $-1{\cdot}675$ for $h/w = 0{\cdot}2$, and $-5{\cdot}400$ for $h/w = 0{\cdot}5$. In particular, we were able via the finite-element procedure to reproduce Figure 2 to well within plotting accuracy.

Since the eigenfunction expansion method gives good results with minimal computer-time expenditure, it is perhaps a preferable technique for the initial flow in a rectangular domain. However, the main reason for use of the finite-element technique is to extend it to the true slumping flow at finite times, where the domain is no longer rectangular. We have done this, using the penalty method within the *Fastflo* package. We chose to use *Fastflo* rather than our own fully-coupled program, because although *Fastflo* has slower convergence with mesh fineness (see Table 1), its overall efficiency is better in terms of total computer time used.

As explained in Section 1, we determine the evolution of the bridge shape in time by first solving the Stokes and continuity equations for the velocity field, which can then be used in the kinematic boundary condition (10) to compute the new free surfaces $y = \eta_{\pm}(x, t)$. However, instead of explicit integration of (10), in order to incorporate automatic remeshing within the time-stepping process, we have chosen to use an equivalent method of solving

$$\mathrm{d}\widetilde{x}/\mathrm{d}t = \widetilde{u} \tag{26}$$

at each mesh node for the new node coordinates $\widetilde{x} = (x, y)$, where $\widetilde{u} = (u, v)$ is the known velocity at the node. We use a fourth-order Runge–Kutta method to solve Equation (26) and then move the (material) nodes to their new positions, to give a new meshed geometry, on which the whole procedure may be repeated.

Figure 5 shows the slumped bridge (and the evolving triangular grid with corner concentrations) for $h/w = 0{\cdot}2$ at $t = 5{\cdot}0h/V$, with V given by (14). For clarity, a mesh of only

248 elements was used, which is in any case quite adequate for graphical accuracy. Actually, Figure 1(b), which was used earlier for illustrative purposes, is also taken from such a computation, at the earlier time $t = 2{\cdot}0h/V$. Both of these figures confirm, especially on the upper free surface, the behaviour suggested by the initial velocity profiles of Figure 4, with a near 'quadratic-squared' shape in the middle parts of the bridge, coupled with a rapid return to the original attachment point near the corner. The upper surface thus possesses fully four inflexion points, being concave upward near the centre and also near both walls, but concave downward in the intermediate regions. Such multiple changes in curvature would be undesirable if this type of slumping flow were to be used in optical manufacturing applications.

Figure 6 shows the slumping velocity (at the point which starts as the centroid of the rectangle), as a function of time, for $h/w = 0{\cdot}2$. The initial value is $-v/V = 1{\cdot}674$, as in Table 1. However, for $t > 0$, the slumping velocity decreases rapidly with time at first, reaching a minimum value of about 37 percent of the initial velocity at $tV/2h = 2{\cdot}5$ when the amount of slump equals a little over two bridge thicknesses, before increasing again, as the central portions of the bridge begin to lose touch with the walls, and enter a state of flow which will eventually culminate in free fall. This type of behaviour is qualitatively typical of that for other aspect ratios. However, when the aspect ratio falls below 0·2, we see a larger decrease in the slumping velocity occurring over a longer time, with the bridge slumping considerably more than three bridge thicknesses before the velocity begins to increase again. For example, with $h/w = 0{\cdot}1$ the velocity drops to 13 percent of its initial value at $tV/2h = 15$, at which time the bridge has slumped nearly four thicknesses. Conversely, when the aspect ratio increases above 0·2, there is a smaller decrease in velocity occurring over a shorter time period, and the bridge slumps a smaller distance in this time. For $h/w = 0{\cdot}5$ the velocity decreases to 73 percent of its original value by $tV/2h = 0{\cdot}24$ before increasing again, at which time the bridge has slumped just one thickness.

The final free-fall state will eventually violate the assumption of neglect of inertia, but so long as inertia remains neglected, the velocity (and acceleration) will appear to approach infinity at some finite time $t = t_C \approx \mu/(\rho g w)$ (unpublished estimate by the present authors, *c.f.* [18, p. 67]). We make no attempt to approach that time in the present computations. All accelerations we compute here are formally very small compared to gravity g, but in this approach to free fall, they will become comparable to g at times just less than the critical time $t = t_C$, and inertia would have to be re-introduced into the problem in order to complete the solution for times close to and greater than t_C.

Figure 7 shows the time taken to slump one bridge thickness $2h$ as a function of aspect ratio. Since the time scale used for this plot is $2h/V$, a unit value would correspond to fall at the constant speed V, which is the initial rate of fall of very thin bridges with small h/w. However, for such thin bridges, even though the initial velocity is close to V, we find a time some 50 percent larger than $2h/V$, since (as in Figure 6) there is already a significant drop in slumping velocity during a slump of one bridge thickness. On the other hand, at larger h/w values, the time to slump one bridge thickness becomes significantly less than $2h/V$, since the slumping velocity then significantly exceeds V, not just initially (see Figure 2), but also at all later times. In fact, for very thick bridges, the time to slump one bridge thickness approaches $2h/\bar{V}$ as h/w becomes large, corresponding to the flow approaching the Poiseuille thick-bridge limit with centroid slumping velocity $\bar{V}$.

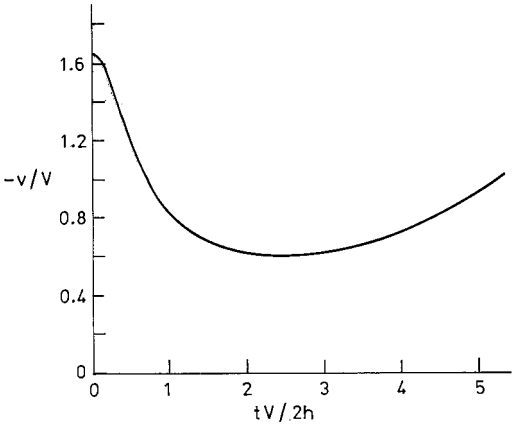

Figure 6. Slumping velocity as a function of time, for $h/w = 0{\cdot}2$.

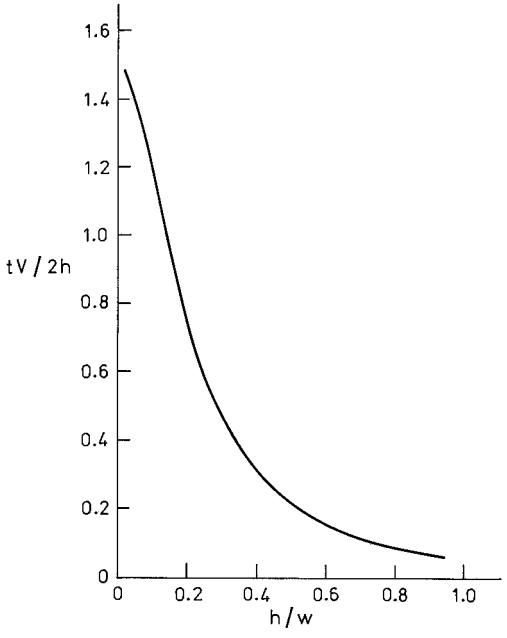

Figure 7. Time to slump one bridge thickness, as a function of aspect ratio.

A. Appendix. Formal thin-bridge asymptotic expansion

In this Appendix, we treat a fully three-dimensional version of the initial slumping problem. The bridge still lies in $|y| < h$ where h is small compared to a length scale w measured in the horizontal (x, z) plane. We expand for small y, which is in effect an expansion in the small parameter $\varepsilon = h/w$, *c.f.* [19].

First we expand all velocities in a power series in y, with the appropriate vertical symmetries, of the form

$$\begin{aligned} u &= yu_1 + y^3u_3 + O(\varepsilon^5), \\ v &= v_0 + y^2v_2 + y^4v_4 + O(\varepsilon^6), \\ w &= yw_1 + y^3w_3 + O(\varepsilon^5), \end{aligned} \tag{27}$$

where all coefficients are general (to-be-determined) functions of x and z. The equations of motion and free-surface boundary conditions provide connections between these coefficients, from which we can eliminate all but v_0.

Continuity ($u_x + v_y + w_z = 0$) demands at once that

$$\begin{aligned} 2v_2 &= -u_{1x} - w_{1z}, \\ 4v_4 &= -u_{3x} - w_{3z}, \end{aligned} \tag{28}$$

and the Stokes equations (5, 6) demand

$$\begin{aligned} p_x &= \mu y(\nabla^2 u_1 + 6u_3) + O(\varepsilon^3), \\ p_y &= -\rho g + \mu(\nabla^2 v_0 + 2v_2) + \mu y^2(\nabla^2 v_2 + 12v_4) + O(\varepsilon^4), \\ p_z &= \mu y(\nabla^2 w_1 + 6w_3) + O(\varepsilon^3), \end{aligned} \tag{29}$$

where the Laplacian ∇^2 involves only x, z derivatives. Hence, the pressure has the expansion

$$p = -\rho g y + \mu y(\nabla^2 v_0 + 2v_2) + \tfrac{1}{3}\mu y^3(\nabla^2 v_2 + 12v_4) + O(\varepsilon^5), \tag{30}$$

where

$$\begin{aligned} \nabla^2 v_{0x} + 2v_{2x} &= \nabla^2 u_1 + 6u_3, \\ \nabla^2 v_{0z} + 2v_{2z} &= \nabla^2 w_1 + 6w_3. \end{aligned} \tag{31}$$

Cross-differentiation of (31) and use of the continuity equations (28) gives a relationship connecting the first three coefficients in the expansion of the vertical velocity component, namely

$$\nabla^4 v_0 + 4\nabla^2 v_2 + 24v_4 = 0. \tag{32}$$

If we were to carry further terms in the expansions (27), we would find a similar relationship between each set of three successive terms, but for the moment (32) will suffice.

Now let us turn to the zero-stress boundary conditions on $y = h$. Zero tangential stress ($u_y + v_x = w_y + v_z = 0$) gives

$$\begin{aligned} u_1 + 3h^2 u_3 + v_{0x} + h^2 v_{2x} + O(\varepsilon^4) &= 0, \\ w_1 + 3h^2 w_3 + v_{0z} + h^2 v_{2z} + O(\varepsilon^4) &= 0, \end{aligned} \tag{33}$$

and cross-differentiation of (33) yields

$$\nabla^2 v_0 - 2v_2 = -h^2(\nabla^2 v_2 - 12v_4) + O(\varepsilon^4). \tag{34}$$

The normal-stress condition ($-p + 2\mu v_y = 0$) gives after some manipulation

$$\frac{\rho g}{\mu} = \nabla^2 v_0 - 2v_2 + h^2(\tfrac{1}{3}\nabla^2 v_2 - 4v_4) + O(\varepsilon^4). \tag{35}$$

Combining (34) and (35), we have to leading order

$$\frac{\rho g}{\mu h^2} = -\tfrac{2}{3}\nabla^2 v_2 + 8v_4 \tag{36}$$

or, using (32) to eliminate v_4,

$$\frac{\rho g}{\mu h^2} = -2\nabla^2 v_2 - \tfrac{1}{3}\nabla^4 v_0. \tag{37}$$

But now we can use the leading-order terms of (34) (*i.e.* left-hand side equals zero) to eliminate v_2, giving finally

$$\frac{\rho g}{\mu h^2} = -\tfrac{4}{3}\nabla^4 v_0. \tag{38}$$

That is, the first approximation $v = v_0(x, z)$ to the vertical velocity satisfies (22).

Concluding remarks

A semi-analytic method has been presented here for determining the initial motion under gravity of a very viscous material spanning the gap between two vertical no-slip walls. To

compute the motion and free-surface shape at subsequent times, we used a numerical method employing finite-element techniques. This latter method is readily used for bridges of arbitrary initial shape with a variety of initial support methods, so that some flows of a character very different from that considered in this paper may be computed. For example, we have used the finite-element code to model extensional flows occurring in drop formation, such as the flow subsequent to inversion of a spoonful of honey, see [20]. A simple extension of the method also permits boundary conditions that change as slumping proceeds, and we are using this in generalisations of the present paper that allow progressive contact with a mould.

Acknowledgements

The authors acknowledge support by the Australian Research Council, which enabled a visit by LWS to Adelaide in 1994 when this work was commenced. They also acknowledge support of YMS under the APA (Industry) scholarship system. An assistance with implementation of the *Fastflo* package by Dr. A.N. Stokes, CSIRO Division of Mathematics and Statistics, is acknowledged.

References

1. L. Smith, R.J. Tillen and J. Winthrop, New directions in aspherics : glass and plastic. In: M.J. Riedl (ed), *Replication and Molding of Optical Components*, Vol. 896, Proceedings of The Society of Photo-Optical Instrumentation Engineers. Washington: Bellingham (1988) pp. 160–166.
2. E.B. Shand, *Glass Engineering Handbook*. New York: McGraw-Hill (1958) 484pp.
3. G.W. Morey, *The Properties of Glass*. New York: Reinhold (1938) 561pp.
4. S.T. Gulati, E.H. Fontana and W.A. Plummer, Disc bending viscometry. *Phys and Chem. of Glasses* 17 (1976) 114–119.
5. H. Rawson, *Properties and Applications of Glass*. New York: Elsevier (1980) 318pp.
6. G.K. Batchelor, *An Introduction to Fluid Dynamics*, Cambridge: Cambridge University Press (1967) 615pp.
7. J.V. Wehausen and E.V. Laitone, Surface Waves. In: S. Flugge (ed), *Handbuch der Physik* Vol. 9. Berlin: Springer (1960) pp. 446–778.
8. B.W. van der Fliert, P.D. Howell and J.R. Ockendon, Pressure-driven flow of a thin viscous sheet. *J. Fluid Mech.* 292 (1995) 359–376.
9. G.D. Smith, *Numerical Solution of Partial Differential Equations: Finite Difference Methods*. Oxford: Clarendon Press (1978) 304pp.
10. S. Timoshenko and J. Goodier, *Theory of Elasticity*, 3rd edn. New York: McGraw-Hill (1970) 567pp.
11. A.P. Hillman and H.E. Salzer, Roots of $\sin z = z$. *Phil. Mag.* 34 (1943) 575.
12. D.D. Joseph, L.D. Sturges and W.H. Warner, Convergence of biorthogonal series of biharmonic eigenfunctions by the method of Titchmarsh. *Arch. Rat. Mech. Anal.* 78 (1982) 223–274.
13. H.K. Moffatt, Viscous and resistive eddies near a sharp corner. *J. Fluid Mech.* 18 (1964) 1–18.
14. S. Timoshenko and S. Woinowsky-Krieger, *Theory of Plates and Shells*. New York: McGraw-Hill (1959) 580pp.
15. A.N. Stokes, *Fastflo* solutions of natural convection problems close to freezing. In: D. Stewart *et al.* (ed), *Computational Techniques and Applications Conference 1993*. Singapore: World Scientific (1994) pp. 446–453.
16. A.N. Stokes, Using conjugate gradient methods in solving the incompressible Navier–Stokes equations. In: A.K. Easton and R.L. May (eds), *Computational Techniques and Applications Conference 1995*. Singapore: World Scientific (1996) pp. 725–732.
17. J.T. Pittman, O.C. Zienkiewicz, R.D. Wood and J.M. Alexander, *Numerical Analysis of Forming Processes*. New York: Wiley (1984) 444pp.
18. A. Kaye, Convected coordinates and elongational flow. *J. Non-Newtonian Fluid Mech.* 40 (1991) 55–77.
19. P.D. Howell, Models for thin viscous sheets. *Euro. J. Appl. Math.* 7 (1996) 321–343.
20. E.O. Tuck, Mathematics of honey on toast. *National Symposium on the Mathematical Sciences*, University of NSW, February 1996. In: R.R. Moore and A.J. van der Poorten (eds), *Multiplying Australia's Potential*. Canberra: Australian Academy of Science (1997).